

Connected-Sea Partons

Keh-Fei Liu,¹ Wen-Chen Chang,² Hai-Yang Cheng,² and Jen-Chieh Peng³

¹*Department of Physics and Astronomy, University of Kentucky, Lexington, Kentucky 40506, USA*

²*Institute of Physics, Academia Sinica, Taipei 11529, Taiwan*

³*Department of Physics, University of Illinois at Urbana-Champaign, Urbana, Illinois 61801, USA*

According to the path-integral formalism of the hadronic tensor, the nucleon sea contains two distinct components called connected sea (CS) and disconnected sea (DS). We discuss how the CS and DS are accessed in the lattice QCD calculation of the moments of the parton distributions. We show that the CS and DS components for $\bar{u}(x) + \bar{d}(x)$ can be extracted by using recent data on the strangeness parton distribution, the CT10 global fit, and the lattice result of the ratio of the strange to $u(d)$ moments in the disconnected insertion. The extracted CS and DS for $\bar{u}(x) + \bar{d}(x)$ have distinct Bjorken x dependence in qualitative agreement with expectation. The analysis also shows that the momentum fraction of the $\bar{u}(x) + \bar{d}(x)$ is about equally divided between CS and DS at $Q^2 = 2.5\text{GeV}^2$. Implications on future global analysis for parton distributions are presented.

PACS numbers: 13.60.Hb, 14.20.Dh, 14.65.Bt, 12.38.Gc

There have been a number of developments in the understanding of the flavor content of the nucleon sea, such as the observation of the light-quark sea difference between \bar{d} and \bar{u} in Deep Inelastic Scattering (DIS) [1] and Drell-Yan processes [2], the extraction of strange quark content $s + \bar{s}$ from semi-inclusive DIS [3], and the lattice QCD calculations of sea quark contributions to nucleon orbital angular momenta [4]. Evidence for the existence of intrinsic sea [5] of the light quarks has also been reported [6].

Many theoretical models, including the meson cloud model, have been suggested for describing the flavor structure of the nucleon sea [7]. In order to gain new insights on the origins of the flavor content of the nucleon sea, it is important to note that, according to the path-integral formalism, there are two distinct sources for nucleon sea, namely, the connected sea (CS) and the disconnected sea (DS) [8, 9]. The CS and DS are expected to have different shapes in their Bjorken- x distribution, as well as distinct quark-flavor dependence. The first direct experimental evidence for the existence of CS came from the observation of large difference in the $\bar{u}(x)$ and $\bar{d}(x)$ distributions [8]. In this paper we show that the two distinct contributions (CS and DS) to the $\bar{u}(x) + \bar{d}(x)$ can be separated based on existing experimental data and input from lattice QCD calculation.

The existence of the connected sea and disconnected sea can be illustrated in the path-integral formalism of the hadronic tensor. In the Euclidean path-integral formalism of the hadronic tensor $W_{\mu\nu}$, there are three gauge invariant and topologically distinct diagrams, as shown in Fig. 1. The various lines in Fig. 1 represent the quark propagators from the source of the nucleon interpolation field at time $t = 0$ to the sink time at t and the currents are inserted at t_1 and t_2 .

We first note that Fig. 1(b), where the quarks propagate backward in time between t_1 and t_2 , corresponds to the connected-sea anti-partons \bar{u}^{cs} and \bar{d}^{cs} . In contrast, the forward propagating quarks in Fig. 1(a) correspond to valence and CS partons u^{v+cs} and d^{v+cs} , where valence is defined as $q^v \equiv q^{v+cs} - \bar{q}^{cs}$ and $q^{cs}(x) \equiv \bar{q}^{cs}(x)$. Finally, Fig. 1(c) gives the DS q^{ds} and \bar{q}^{ds} for $q = u, d, s, c$, since it contains

both forward and backward propagating quarks. The nomenclature of connected and disconnected seas follows those in the time-ordered perturbation theory – CS is the higher Fock-state component in the Z-graph where the quark lines are connected and the DS corresponds to the vacuum polarization.

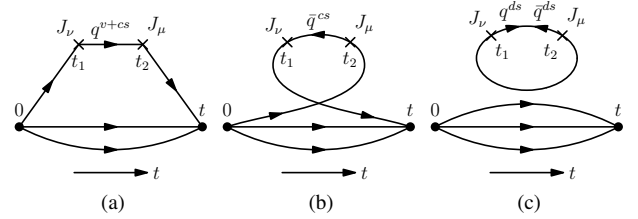


FIG. 1: Three gauge invariant and topologically distinct diagrams in the Euclidean path-integral formalism of the nucleon hadronic tensor in the large momentum frame. In between the currents at t_1 and t_2 , the parton degrees of freedom are (a) the valence and CS partons q^{v+cs} , (b) the CS anti-partons \bar{q}^{cs} , and (c) the DS partons q^{ds} and anti-partons \bar{q}^{ds} with $q = u, d, s$, and c . Only u and d are present in (a) and (b).

It is clear from Fig. 1 that the two sources of the sea quarks, CS and DS, have interesting quark-flavor dependence. For example, while u and d have both CS and DS, s and c have only DS. The small mass difference between the u and d quarks implies that the DS cannot account for the large \bar{d}/\bar{u} difference observed in the DIS and Drell-Yan experiments. Rather, this difference must originate primarily from the CS diagram of Fig. 1(b) due to the fact that there are two u -valence quarks but only one d . The absence of the CS component for the strange and charm quarks also implies that any difference between $s(x)$ and $\bar{s}(x)$ (or $c(x)$ and $\bar{c}(x)$) distributions, as predicted in meson cloud [10] and intrinsic sea [11] models, must come from the DS diagram of Fig. 1(c). The classification of parton distribution functions in terms of flavor, CS and DS is given in Table I.

The CS and DS are also expected to have distinct distributions at the small- x region. Since there is only reggeon exchange for the flavor non-singlet valence and CS, the valence

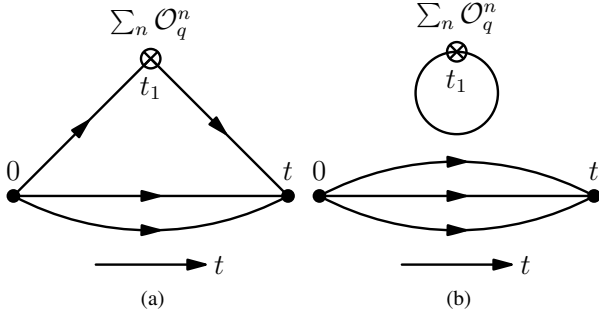


FIG. 2: The three-point functions after the short-distance expansion of the hadronic tensor from Fig. 1. (a) The connected insertion (CI) is derived from Fig. 1(a) and Fig. 1(b). (b) The disconnected insertion (DI) originates from Fig. 1(c). \mathcal{O}_q^n are local operators which are the same as derived from OPE.

TABLE I: Classification of PDF in the nucleon for different flavors.

Valence and Connected Sea			
$u^{v+cs}(x)$	$\bar{u}^{cs}(x)$	$d^{v+cs}(x)$	$\bar{d}^{cs}(x)$
Disconnected Sea			
$u^{ds}(x) + \bar{u}^{ds}(x)$	$d^{ds}(x) + \bar{d}^{ds}(x)$	$s(x) + \bar{s}(x)$	$c(x) + \bar{c}(x)$

and CS partons is $q^{v+cs}(x)$, $\bar{q}^{cs}(x) \xrightarrow{x \rightarrow 0} \propto x^{-1/2}$ at small x . For the DS partons, there is flavor-singlet pomeron exchange, thus its small- x behavior is $q^{ds}(x)$, $\bar{q}^{ds}(x) \xrightarrow{x \rightarrow 0} \propto x^{-1}$. In addition, there are also meson cloud contributions which are prominent in the medium- x range. Partons with these different small- x behaviors are considered as extrinsic and intrinsic distributions for charm [5] and the light quarks [6]. The distinct flavor and x -dependence of CS and DS remain to be checked experimentally.

Under the short-distance expansion of the hadronic tensor between the current insertions in the path-integral formalism (*N.B.* This corresponds to operator product expansion (OPE) in the canonical formalism), Fig. 1(a) and Fig. 1(b) become the connected insertions (CI) in Fig. 2(a) for a series of local operators $\sum_n \mathcal{O}_q^n$ in the three-point functions from which the nucleon matrix elements for the moments of the CI are obtained. Here the flavor $q = u, d$ are the valence flavors from the interpolation field. By the same token, the disconnected four-point functions in Fig. 1(c) become the disconnected insertions (DI) in Fig. 2(b) for the three-point functions to obtain the DI moments. Here $q = u, d, s, c$ are the DS flavors in the DI. The main advantage of the path-integral formalism over the canonical formalism is that the parton degrees of freedom are tied to the topology of the quark skeleton diagrams in Figs. 1(a), 1(b), and 1(c) so that the CS and the DS can be separated. Lattice QCD can access these three-point functions for the CI and DI which separately contain the CS and DS and calculations of the moments of the unpolarized and polarized PDFs for the quarks [12] and glue [4] have been carried out.

Unfortunately, lattice calculations cannot calculate the parton x -distributions directly [9], only moments are accessible.

To delineate the flavor and x dependence of the parton distributions, it is important to have the CS and DS separated in the global fitting as they evolve differently in Q^2 [9]. Once they are separated in one Q^2 , they will remain separated so that they can be used to fit experiments or make predictions at other Q^2 . While the difference of $\bar{u}^{cs}(x)$ and $\bar{d}^{cs}(x)$ is obtained from the E866 Drell-Yan [2] and HERMES semi-inclusive [13] measurements of $\bar{d}(x) - \bar{u}(x)$, there is not yet an established way to directly obtain $\bar{u}^{cs}(x) + \bar{d}^{cs}(x)$ from experiments. We shall show how to achieve this with a combination of experimental results and a lattice calculation of $\langle x \rangle$ for the DI in Fig. 2(b).

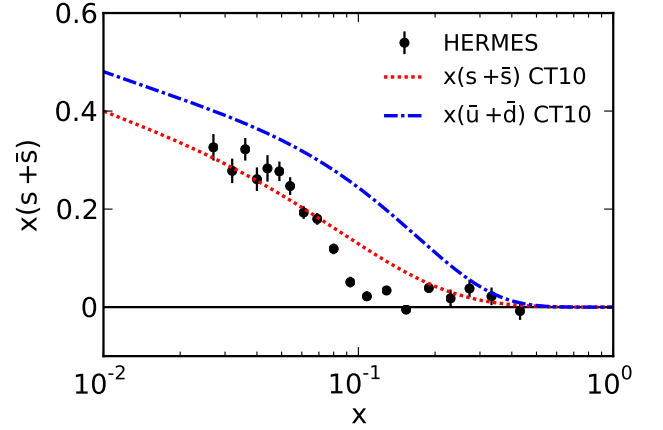


FIG. 3: The strange quark PDF from HERMES semi-inclusive DIS experiment of kaon production on deuteron. It is compared to CT10 results.

Recent HERMES semi-inclusive DIS experiment of kaon production on deuteron [3] has produced the strangeness parton distribution function $s(x) + \bar{s}(x)$ at $Q^2 = 2.5 \text{ GeV}^2$ which is shown in Fig. 3. One notable feature is that the values at medium x around 0.1 are quite different from those obtained from the global fit of CT10 [14] (also drawn in Fig. 3), which did not include the HERMES data in the fit. Since s and \bar{s} are entirely due to DS, the HERMES $s(x) + \bar{s}(x)$ data provide valuable information on the shape of the x -distribution for DS, which is not available from the lattice calculation.

We can now proceed to separate the CS and DS components of the $\bar{u} + \bar{d}$ sea with the following approach. First, we shall make the plausible ansatz that the distribution of $\bar{u}^{ds}(x) + \bar{d}^{ds}(x)$ is proportional to that of $s(x) + \bar{s}(x)$ and the proportionality is $\frac{1}{R}$, i.e., $\bar{u}^{ds}(x) + \bar{d}^{ds}(x) = \frac{1}{R}(s(x) + \bar{s}(x))$. As discussed below, a recent lattice calculation has obtained $R = 0.857 \pm 0.040$. We can then extract $\bar{u}^{cs}(x) + \bar{d}^{cs}(x)$ from the difference of the CT10 result on $\bar{u}(x) + \bar{d}(x)$ and the HERMES data weighted with $\frac{1}{R}$,

$$\bar{u}^{cs}(x) + \bar{d}^{cs}(x) = \bar{u}(x) + \bar{d}(x) - \frac{1}{R}(s(x) + \bar{s}(x)) \quad (1)$$

at $Q^2 = 2.5 \text{ GeV}^2$. The $\bar{u}(x) + \bar{d}(x)$ in Eq. 1 can be taken from the recent CT10 PDF.

A recent lattice calculation [15] of the momentum fraction $\langle x \rangle$ for the strange and $u(d)$ in the DI was carried out with 2 + 1-flavor dynamical fermion gauge configurations with the improved gauge and Wilson fermion (clover) actions. The ratio of the momentum fraction between the strange and the $u(d)$ in the DI, where multiplicative renormalization constants and some systematic errors cancel, is extrapolated to the chiral limit with the lowest pion mass at 600 MeV and the result is

$$R = \frac{\langle x \rangle_{s+\bar{s}}}{\langle x \rangle_{u+\bar{u}}(DI)} = \frac{\langle x \rangle_{s+\bar{s}}}{\langle x \rangle_{\bar{u}^{ds}+\bar{d}^{ds}}} = 0.857(40). \quad (2)$$

The second equality is based on the premises of isospin symmetry of the DS, i.e., $\bar{u}^{ds} = \bar{d}^{ds}$ and that the parton-antiparton difference is negligible in the DS, i.e., $u^{ds} = \bar{u}^{ds}$.

It is interesting to note that the ratio R in Eq. (2) is close to unity, much larger than the globally fitted ratio of $\frac{\langle x \rangle_{s+\bar{s}}}{\langle x \rangle_{\bar{u}+\bar{d}}} \sim 0.5$ as evidenced in the CT10 results in Fig. 3. The difference is due to the fact that $\bar{u} + \bar{d}$ has an additional contribution from CS which the strange partons do not have. Moreover, the ratio $R = 0.857$ is very close to that of the CT10 fit at small x (e.g., $x < 2 \times 10^{-2}$). This is consistent with the recent ATLAS measurement of the inclusive W and Z productions, where the strange-to-down quark ratio was determined to be $1.00^{+0.25}_{-0.28}$ at $x = 0.023$ and $Q^2 = 1.9 \text{ GeV}^2$ [16]. Since partons at small x are dominated by the DS, this shows that both the ratio of $(s(x) + \bar{s}(x))/(\bar{u}^{ds}(x) + \bar{d}^{ds}(x))$ of CT10 (and ATLAS) at small x and the ratio of their second moments from the lattice are practically the same. This supports the ansatz that $\bar{u}^{ds}(x) + \bar{d}^{ds}(x) = \frac{1}{R}(s(x) + \bar{s}(x))$.

We plot the distribution function evaluated with Eq. (1), multiplied by the momentum fraction, i.e., $x(\bar{u}(x) + \bar{d}(x) - \frac{1}{R}(s(x) + \bar{s}(x)))$ in Fig. 4 together with $x(\bar{d}(x) - \bar{u}(x))$ from E866 Drell-Yan measurement [2] at $Q^2 = 54 \text{ GeV}^2$ and from SIDIS HERMES measurement [13] at $\langle Q^2 \rangle = 2.3 \text{ GeV}^2$. We see that $x(\bar{u}^{cs}(x) + \bar{d}^{cs}(x))$ from Eq. (1) is peaked at medium $x \sim 0.1$, the same way as $x(\bar{d}(x) - \bar{u}(x))$ from E866 and HERMES. This is consistent with the expectation that the small- x of CS, like the valence, behaves as $x^{-1/2}$ as we alluded to earlier; so that, when CS is multiplied with x , it would be peaked at medium x , in contrast to that of the DS, e.g., $x(s(x) + \bar{s}(x))$ in Fig. 3. Furthermore, we note that $x(\bar{u}^{cs}(x) + \bar{d}^{cs}(x))$ is generally larger than $x(\bar{d}(x) - \bar{u}(x))$ in this x -range as it should and is larger by a factor ~ 4 at the peak.

We also plot $x(\bar{u}(x) + \bar{d}(x) - \frac{1}{R}(s(x) + \bar{s}(x)))$, $x(\bar{u}^{ds}(x) + \bar{d}^{ds}(x) - \frac{1}{R}(s(x) + \bar{s}(x)))$ and $x(\bar{u}(x) + \bar{d}(x))$ from CT10 in Fig. 5 to show that the CS and DS have very different x -dependence. The different shapes of CS and DS are in good agreement with the expectation discussed earlier. This agreement lends support for the approach we adopted. It is interesting to note that should a very different value of R be used, the x -dependence of CS and DS would no longer agree with

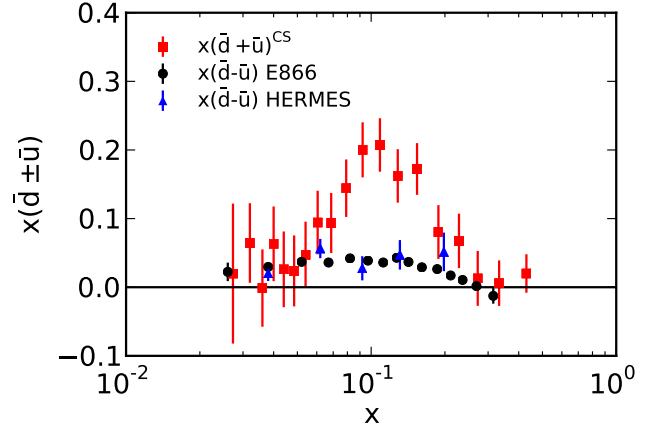


FIG. 4: $x(\bar{d}^{cs}(x) + \bar{u}^{cs}(x))$ obtained from Eq. (1) is plotted together with $x(\bar{d}(x) - \bar{u}(x))$ from E866 Drell-Yan experiment [2] and from SIDIS HERMES experiment [13].

expectation. In particular, if R were appreciably larger than the present value of 0.857, Eq. (1) would lead to a CS whose small x behavior would be $\sim x^{-1}$ which is inconsistent with the fact that CS is from the connected insertion. In this case, $x(\bar{u}^{cs}(x) + \bar{d}^{cs}(x))$ would approach a constant as $x \rightarrow 0$ as opposed to zero, as illustrated in Fig. 5. On the other hand, if R were appreciably smaller than 0.857, the CS from Eq. (1) would turn out to be negative and this would not be commensurate with the probability interpretation for CS.

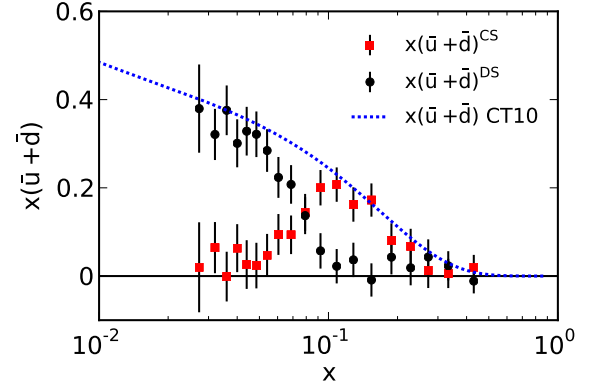


FIG. 5: $x(\bar{u}^{cs}(x) + \bar{d}^{cs}(x))$ obtained from Eq. (1) is plotted together with $x(\bar{u}(x) + \bar{d}(x))$ from CT10 and $\frac{1}{R}x(s(x) + \bar{s}(x))$ which is taken to be $x(\bar{u}^{ds}(x) + \bar{d}^{ds}(x))$.

We can also calculate the momentum fractions carried by the CS and DS of $\bar{u} + \bar{d}$ as follows. First, the total contributions of $\bar{u} + \bar{d}$, i.e., $\langle x \rangle_{\bar{d}+\bar{u}} = \int_0^1 dx x(\bar{d}(x) + \bar{u}(x))$ for the global fittings of CT10, CTEQ6 [17] and MSTW08 [18] are listed in Table II. Here, the uncertainty of a specific PDF function is estimated by varying the range of the calculated quantity with input from the alternative eigenvectors of the

TABLE II: Values of various moments using the HERMES data, the lattice QCD result, and three different PDFs at $Q^2 = 2.5 \text{ GeV}^2$.

	CT10	CTEQ6	MSTW08
$\langle x \rangle_{\bar{d}+\bar{u}}$	0.0639(14)	0.0614(14)	0.0690(11)
$\langle x \rangle_{\bar{d}^{cs}+\bar{u}^{cs}}$	0.0294(54)	0.0281(54)	0.0347(53)
$\langle x \rangle_{\bar{d}^{ds}+\bar{u}^{ds}}$	0.0344(52)	0.0332(52)	0.0342(52)
$\frac{\langle x \rangle_{\bar{d}^{cs}+\bar{u}^{cs}}}{\langle x \rangle_{\bar{d}^{ds}+\bar{u}^{ds}}}$	0.86(29)	0.85(30)	1.02(32)

PDF and is quoted in the parentheses. The CS contributions $\langle x \rangle_{\bar{d}^{cs}+\bar{u}^{cs}}$ in Table II are then obtained from Eq. 1 with inputs of $\bar{d}(x) + \bar{u}(x)$ from the different PDFs and integrated over the range $0.025 < x < 0.48$ plus a small contribution outside this range which is estimated to be 2% from the fractional contribution to $x(\bar{d}(x) - \bar{u}(x))$ outside this range based on CT10. The total uncertainty includes the contributions from HERMES data, the lattice calculation of R , the PDF, and the unmeasured x region. The corresponding $\langle x \rangle_{\bar{d}^{ds}+\bar{u}^{ds}}$ in Table II is taken to be the difference between the respective $\langle x \rangle_{\bar{d}+\bar{u}}$ and $\langle x \rangle_{\bar{d}^{cs}+\bar{u}^{cs}}$. Finally, we give the ratio $\frac{\langle x \rangle_{\bar{d}^{cs}+\bar{u}^{cs}}}{\langle x \rangle_{\bar{d}^{ds}+\bar{u}^{ds}}}$. It is interesting that this ratio is close to unity, showing that the momentum fraction of $\bar{d} + \bar{u}$ is about equally divided between the CS and the DS at this low Q^2 . Future lattice calculations could provide a direct check of the second moment of $\bar{u}^{ds}(x) + \bar{d}^{ds}(x)$ shown in Table II.

In order to gain deeper and more precise understanding of the PDF in terms of their flavor, x and Q^2 dependence, it is essential to have the CS and DS separately accommodated in the extended evolution equations. Only then will they remain separated at different Q^2 to facilitate global fitting, as they evolve differently with the CS evolving like the valence [9]. This will have an impact on the gluon distribution as well. Furthermore, only with CS and DS separated, will one be able to address the flavor dependence, i.e., $\bar{u}^{ds} \neq \bar{d}^{ds}$ and parton-antiparton difference of the u and d partons in the DS and check the validity of the ansatz that $\bar{u}^{ds}(x) + \bar{d}^{ds}(x)$ is proportional to $s(x) + \bar{s}(x)$. As the lattice calculations are getting more refined when the physical pion mass, continuum limit, and large volume limit are approached, they could serve as valuable constraints for the parton moments. In particular, higher moments in CI will help separate the valence and CS parton distributions in the global analysis and the DI calculation of the fourth moment for the strange and u/d (i.e., $\langle x^3 \rangle_u(DI) = \int dx x^3 (u^{ds}(x) + \bar{u}^{ds}(x))$) can be used to gauge how good the proportionality assumption is about their distributions.

In summary, we have shown that there are two sources for the sea partons, the CS and DS, based on the path-integral formalism of the hadronic tensor. While the u and d have both CS and DS contributions, the s and c partons are from the

DS only. We also expect that the CS and DS have different x distributions. These different flavor and x dependence offer the possibility of disentangling the CS from the DS. We first show that the expectation for the dominance of DS at small x is supported by the good agreement between the lattice calculation of $R = \frac{\langle x \rangle_{s+\bar{s}}}{\langle x \rangle_{u+\bar{u}}(DI)} = 0.857(40)$ and the ratio of $x(s(x) + \bar{s}(x))$ from the HERMES data [3] to $x(\bar{u}(x) + \bar{d}(x))$ from CT10 at small x (e.g., $x < 2 \times 10^{-2}$) as shown in Fig 3. Given this agreement, we show how the HERMES data on strangeness parton distributions, the lattice calculation of R , and the CT10 global fit of $\bar{d} + \bar{u}$, can determine the separate CS and DS contributions in $\bar{u} + \bar{d}$. We stress that the ansatz of the proportionality between $\bar{u}^{ds}(x) + \bar{d}^{ds}(x)$ and $s(x) + \bar{s}(x)$ should be checked with lattice calculation of R with light dynamical fermions as well as the ratio for $\langle x^3 \rangle$ in the DI. Future global analysis of PDF should have CS and DS separated in the fitting and in the evolution equations.

This work is partially supported by U.S. Department of Energy grant DE-FG05-84ER40154, National Science Foundation and the National Science Council of the Republic of China. We thank C.P. Yuan for fruitful discussion.

-
- [1] P. Amaudruz *et al.* (New Muon Collaboration), Phys. Rev. Lett. **66**, 2712 (1991).
 - [2] R.S. Towell *et al.* (FNAL E866/NuSea Collaboration), Phys. Rev. **D64**, 052002 (2001).
 - [3] A. Airapetian *et al.* (HERMES), Phys. Lett. **B666**, 446 (2008).
 - [4] K.F. Liu *et al.*, PoS **LATTICE2011**, 164 (2011), [arXiv:1203.6388].
 - [5] S.J. Brodsky, P. Hoyer, C. Peterson, and N. Sakai, Phys. Lett. B **93**, 451 (1980).
 - [6] W.C. Chang and J.C. Peng, Phys. Rev. Lett. **106**, 252002 (2011); Phys. Lett. **B 704**, 197 (2011).
 - [7] G. T. Garvey and J. C. Peng, Prog. Part. Nucl. Phys. **47**, 203 (2001).
 - [8] K.F. Liu and S.J. Dong, Phys. Rev. Lett. **72**, 1790 (1994).
 - [9] K.F. Liu, Phys. Rev. **D62**, 074501 (2000).
 - [10] A.I. Signal and A.W. Thomas, Phys. Lett. **B191**, 205 (1987).
 - [11] S.J. Brodsky and B.Q. Ma, Phys. Lett. **B381**, 317 (1996).
 - [12] J. D. Bratt *et al.* (LHPC), Phys. Rev. **D82**, 094502 (2010); M. Göckeler *et al.* (QCDSF/UKQCD), PoS **Lat2010**, 163 (2010); M. Deka *et al.* (χ QCD), Phys. Rev. **D79**, 094502 (2009).
 - [13] A. Ackerstaff *et al.* (HERMES), Phys. Rev. Lett. **81**, 5519 (1998).
 - [14] H.L. Lai, M. Guzzi, J. Huston, Z. Li, P.M. Nadolsky, J. Pumplin, C.-P. Yuan, Phys. Rev. **D82**, 074024 (2010), [arXiv:1007.2241].
 - [15] T. Doi *et al.* (χ QCD), PoS **LATTICE2008**, 163 (2008).
 - [16] The ATLAS Collaboration, Phys. Rev. Lett. **109**, 012001 (2012).
 - [17] J. Pumplin, D.R. Stump, J. Huston, H.L. Lai, P.M. Nadolsky, W.K. Tung, JHEP **0207**, 012 (2002).
 - [18] A.D. Martin, W.J. Stirling, R.S. Thorne, G. Watt, Eur. Phys. J. **C63**, 189 (2009).